

## Appearance of hyperons in neutron stars

H. Ćapo,<sup>1,\*</sup> B.-J. Schaefer,<sup>2,†</sup> and J. Wambach<sup>1,3</sup>

<sup>1</sup>*Institut für Kernphysik, TU Darmstadt, Schloßgartenstr. 9, D-64289 Darmstadt, Germany*

<sup>2</sup>*Institut für Physik, Karl-Franzens-Universität Graz, Universitätsplatz 5, A-8010 Graz, Austria*

<sup>3</sup>*Gesellschaft für Schwerionenforschung mbH, Planckstr. 1, D-64291 Darmstadt, Germany*

(Received 22 November 2008; revised manuscript received 3 December 2009; published 19 March 2010)

By employing a recently constructed hyperon-nucleon potential the equation of state of  $\beta$ -equilibrated and charge neutral nucleonic matter is calculated. The hyperon-nucleon potential is a low-momentum potential which is obtained within a renormalization group framework. Based on the Hartree-Fock approximation at zero temperature the densities at which hyperons appear in neutron stars are estimated. For several different bare hyperon-nucleon potentials and a wide range of nuclear matter parameters it is found that hyperons in neutron stars are always present. These findings have profound consequences for the mass and radius of neutron stars.

DOI: [10.1103/PhysRevC.81.035803](https://doi.org/10.1103/PhysRevC.81.035803)

PACS number(s): 13.75.Ev, 21.65.Mn, 26.60.-c

### I. INTRODUCTION

Neutron stars (NS) are compact objects with interior densities of several times normal nuclear density. The precise and detailed structure and composition of the inner core of a NS is not known at present. Several possibilities such as mixed phases of quark and nuclear matter, kaon, or pion condensates or color superconducting quark phases are under debate.

In the present work the influence of hyperons with strangeness  $S = -1$  ( $\Lambda$ ,  $\Sigma^-$ ,  $\Sigma^0$ , and  $\Sigma^+$ ) on the composition and structure of a NS is investigated. In this context the central and essential quantity to be analyzed is the equation of state (EOS). The EOS determines various NS observables such as the mass range or the mass-radius relation of the star. The composition and structure of neutron and also of protoneutron stars have been investigated in detail with a wide range of EOS for dense nuclear matter [1,2]. The emergence of hyperons for increasing nucleon densities has been suggested in the pioneering work of Ref. [3]. Since then the impact of hyperons on dense matter has been studied extensively with different approaches, see, e.g., Refs. [1,4–9]. Unfortunately, the details of the hyperon-nucleon ( $YN$ ) interaction and even more of the hyperon-hyperon ( $YY$ ) interaction are known only poorly. The limited amount of available experimental data enables the construction of many different potentials. For example, the Nijmegen group has proposed six different potentials which all describe the low-energy data such as phase shifts equally well; see, e.g., Ref. [10].

We wish to explore the differences between the available  $YN$  interactions and their influences on the appearance of hyperons in neutron stars. For this purpose the hyperon  $YN$  threshold densities are calculated. Since the  $\Sigma^0$  and  $\Sigma^+$  hyperons are heavier than the  $\Lambda$  and  $\Sigma^-$  hyperons they typically appear later. Hence, we will focus on the  $\Lambda$  and  $\Sigma^-$  hyperons in the following.

The article is organized as follows: In Sec. III the EOS of dense matter including hyperons are calculated. For the pure nucleonic part of the EOS a parametrization is used. A central

quantity which enters the EOS is the single-particle potential. The derivation of the single-particle potential for hyperons is given in Sec. II. The requirements which are necessary for equilibrium are discussed in subsection IV A and the results are collected in subsection IV B. The next section Sec. V shows the calculations of neutron stars with and without hyperons. Finally, the work is summarized and conclusions are drawn in Sec. VI.

### II. SINGLE-PARTICLE POTENTIALS

Single-particle potentials are a useful and important tool to determine the density at which hyperons begin to appear in baryonic matter. They can be obtained from an effective low-momentum  $YN$  potential  $V_{\text{low } k}$  [11,12] in the Hartree-Fock approximation. Details concerning the derivation of the  $YN$  single-particle potentials in this approximation can be found in Ref. [13]. With these single-particle potentials the chemical potentials and particle energies in  $\beta$ -equilibrated matter can be calculated. This allows us to compute the threshold densities for the appearance of a given hyperon species and to establish the concentrations of all particles in dense matter at a given density. In the process we will also determine the EOS for the mixture of leptons and baryons (electrostatic interactions are neglected because their energies are orders of magnitude smaller than the other interaction energies).

Our many-body scheme employs several “bare”  $YN$  interactions as input for the  $V_{\text{low } k}$  calculation: the original Nijmegen soft-core model NSC89 [14], a series of new soft-core Nijmegen models NSC97a-f [10], a recent model proposed by the Jülich group J04 [15], and chiral effective field theory ( $\chi$ EFT) [16]. The first three models are formulated in the conventional meson-exchange (OBE) framework, while the  $\chi$ EFT is based on chiral perturbation theory (for recent reviews see, e.g., Refs. [17–19]). In the  $\chi$ EFT approach a cutoff  $\Lambda_{\chi\text{EFT}}$  enters which we fix to  $\Lambda_{\chi\text{EFT}} = 600$  MeV and label the results obtained by  $\chi\text{EFT}600$ .

In general, the effective low-momentum  $YN$  interaction, the  $V_{\text{low } k}$  for hyperons, is obtained by solving a renormalization group equation. The starting point for the construction of

\*haris@crunch.ikp.physik.tu-darmstadt.de

†bernd-jochen.schaefer@uni-graz.at

the  $V_{\text{low } k}$  is the half-on-shell  $T$  matrix. An effective low-momentum  $T_{\text{low } k}$  matrix is then obtained from a nonrelativistic Lippmann-Schwinger equation in momentum space by introducing a momentum cutoff  $\Lambda$  in the kernel. Simultaneously, the bare potential is replaced with the corresponding low-momentum potential  $V_{\text{low } k}$ ,

$$\begin{aligned} T_{\text{low } k, y' y}^{\alpha' \alpha}(q', q; q^2) \\ = V_{\text{low } k, y' y}^{\alpha' \alpha}(q', q) \\ + \frac{2}{\pi} \sum_{\beta, z} P \int_0^\Lambda dl l^2 \frac{V_{\text{low } k, y' z}^{\alpha' \beta}(q', l) T_{\text{low } k, z y}^{\beta \alpha}(l, q; q^2)}{E_y(q) - E_z(l)}. \end{aligned} \quad (1)$$

The on-shell energy is denoted by  $q^2$  while  $q', q$  are relative momenta between a hyperon and nucleon. The labels  $y, y', z$  indicate the particle channels, and  $\alpha, \alpha', \beta$  denote the partial waves, e.g.,  $\alpha = LSJ$  where  $L$  is the angular momentum,  $J$  the total momentum, and  $S$  the spin. In Eq. (1) the energies in the denominator are given by

$$E_y(q) = M_y + \frac{q^2}{2\mu_y}, \quad (2)$$

with the reduced mass  $\mu_y = M_Y M_N / M_y$ , where  $M_y$  is the total mass of the hyperon-nucleon system,  $M_y = M_Y + M_N$ . Finally, the effective low-momentum  $V_{\text{low } k}$  is defined by the requirement that the  $T$  matrices are equivalent for all momenta below the cutoff  $\Lambda$ . Details for several bare  $YN$  potentials within the RG framework can be found in Refs. [11,12].

From the different effective  $V_{\text{low } k}$  interactions we calculate the single-particle potential  $U_b(p)$  of a baryon  $b \in \{p, n, \Lambda, \Sigma^-, \Sigma^0, \Sigma^+, \Xi^-, \Xi^0\}$  with three-momentum  $p = |\vec{p}|$ . In general, it is defined as the diagonal part in spin and flavor space of the proper self-energy for the corresponding single-particle Green's function. In the Hartree-Fock (HF) approximation for a uniform system it represents the first-order interaction energy of the baryon with the filled Fermi sea. It is evaluated as the diagonal elements of the low-momentum potential matrix,  $V_y^\alpha(q)$ , where an evident short-hand labeling for the diagonal elements has been introduced [cf. Eq. (1)]. Note, that the relative momentum is given by  $q = |\vec{p} - \vec{p}'|$  and the particle channel index is given by  $y = bb'$ . In the HF approximation the single-particle potential has two contributions: the (direct) Hartree- and the (exchange) Fock-term [20]

$$U_b(p) = \sum_{\vec{p}' \alpha b'} \left( V_y^\alpha(q) \Big|_{\text{direct}} + (-1)^{L+S} V_y^\alpha(q) \Big|_{\text{exchange}} \right). \quad (3)$$

In this expression the diagonal elements of the nucleon-nucleon ( $NN$ ) interaction is also included. In principle, an effective low-momentum potential for the  $NN$  interaction is also known but we will use for the  $NN$  sector a parametric Ansatz to be discussed later [see Eq. (9)].

The density dependence for several  $\Lambda$  potentials at rest in symmetric nuclear matter (no hyperons present) is shown in Fig. 1. The square represents the generally expected empirical depth of  $U_\Lambda(p=0) \approx -30$  MeV. While most of the potentials used can reproduce this value, the Jülich potential (J04)

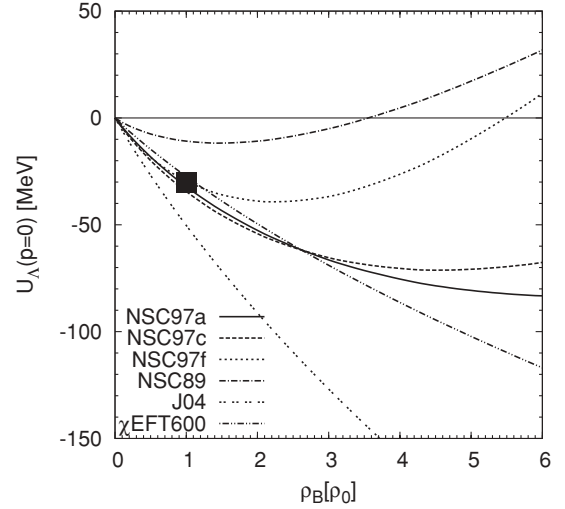


FIG. 1. Density dependence of  $\Lambda$  single-particle potentials for various hyperon-nucleon interactions in symmetric nuclear matter.

yields a stronger binding while the old Nijmegen potential (NSC89) underestimates the binding. All other potentials agree up to the saturation density. However, with increasing density, the differences grow, leading to different bindings at rest. This will have consequences for the predictions of the  $\Lambda$  hyperon concentration in dense nuclear matter. A comparison with other works (Refs. [10,21,22]) shows some differences but mostly yields similar results.

Figure 2 shows the density dependence of several  $\Sigma^-$  potentials at rest in symmetric nuclear matter similar to Fig. 1. No agreement of the various  $U_{\Sigma^-}$  potentials over the density range considered is seen. Compared with a  $G$ -matrix calculation a stronger binding for the  $\Sigma^-$  single-particle potential is obtained. In Ref. [13] further details concerning the hyperon single-particle potentials can be found.

For constructing the total energy/particle one has to distinguish which part of the total single-particle potential comes from the in-medium nucleon interaction and which from the

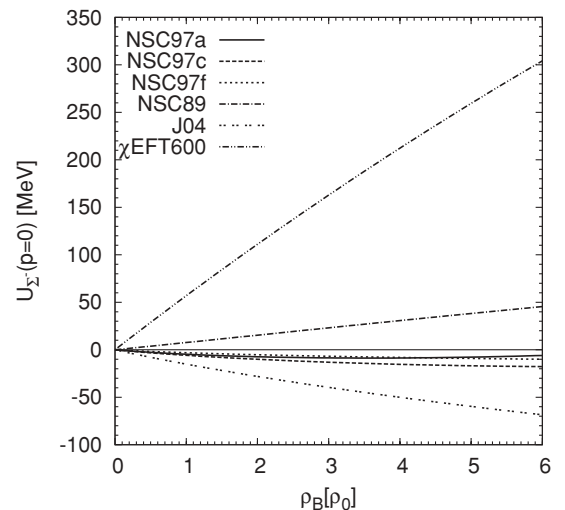


FIG. 2. Same as in Fig. 1 but for the  $\Sigma^-$  hyperon.

hyperons. For this purpose, the single-particle potential can be split into a nucleonic and hyperonic contribution

$$U_b(p) = U_b^N(p) + U_b^Y(p), \quad (4)$$

where the first one,  $U_b^N(p)$ , denotes the baryon interacting with a nucleon and the second one,  $U_b^Y(p)$ , means the baryon interaction with a hyperon. Note, that the baryon can either be a nucleon or a hyperon. Accordingly, the nucleonic contribution is calculated from Eq. (3) via

$$U_b^N(p) = \sum_{\substack{\vec{p}'\alpha \\ b'=p,n}} \left[ V_y^\alpha(q) \Big|_{\text{direct}} + (-1)^{L+S} V_y^\alpha(q) \Big|_{\text{exchange}} \right] \quad (5)$$

and analogously for the hyperonic contribution.

### III. EQUATION OF STATE

By means of the single-particle potential the total energy per particle,  $E/A$ , can be easily calculated. It is given by the total energy of a baryon of mass  $M_b$  and its kinetic and potential energy  $U_b(p)$  divided by the total baryon number density  $\rho_B$ :

$$E/A = \frac{2}{\rho_B} \sum_b \int_0^{k_{F_b}} \frac{d^3 p}{(2\pi)^3} \left[ M_b + \frac{p^2}{2M_b} + \frac{1}{2} U_b(p) \right]. \quad (6)$$

The potential  $U_b(p)$  describes the average field which acts on these baryons due to their interaction with the medium. The baryon Fermi momentum  $k_{F_b}$  is given by

$$k_{F_b}^3 = 3\pi^2 x_b \rho_B \quad (7)$$

with the baryon fraction ratio  $x_b = \rho_b/\rho_B$  for baryon  $b$ .

It is well-known that nonrelativistic many-body calculations, based on purely two-body forces, fail to reproduce the properties of nuclear matter at saturation density. This is also the case in the present work. In order to proceed we replace the purely nucleonic contributions (without the influence of the hyperons) by an analytic parametrization developed by Heiselberg and Hjort-Jensen [23]. This replacement makes the study of hyperons more robust since the  $NN$  sector can be controlled more easily.

From Eq. (6) the purely nucleonic contribution to the energy per particle reads

$$E_{NN}/A_N = \frac{2}{\rho_N} \sum_N \int_0^{k_{F_N}} \frac{d^3 p}{(2\pi)^3} \left[ M_N + \frac{p^2}{2M_N} + \frac{1}{2} U_N^N(p) \right], \quad (8)$$

where the single-particle potential  $U_N^N(p)$  only contains the nucleonic contribution, cf. Eq. (5). However, instead of using the Hartree-Fock expression we employ the following parametrization

$$E_{NN}/A_N = M_N - E_0 u \frac{u - 2 - \delta}{1 + u\delta} + S_0 u^\gamma (1 - 2x_p)^2, \quad (9)$$

where  $u = \rho_N/\rho_0$  denotes the ratio of the total nucleonic density  $\rho_N = (x_p + x_n)\rho_B$  to the nuclear saturation density  $\rho_0 = 0.16 \text{ fm}^{-3}$ . The corresponding proton and neutron fraction are denoted by  $x_p$  and  $x_n$ . The parameters  $E_0$ ,  $\delta$ ,  $S_0$  are

related to properties of nuclear matter at saturation density, i.e.,  $E_0$  is the binding energy per nucleon at saturation density while  $S_0$  and  $\delta$  are connected to the symmetry energy and incompressibility, respectively.

As mentioned in the previous section, cf. Eq. (4), we can separate the potential contribution of nucleons into one coming from the interaction with other nucleons  $U_N^N(p)$  and one coming from the interaction with hyperons  $U_N^Y(p)$ . The latter does not contribute to the purely nucleonic EOS when we consider symmetric matter only. However, in the next section, when we investigate hyperons such terms are considered.

The parametrization (9) is fitted to the energy per particle in symmetric matter obtained from variational calculations with the Argonne  $V_{18}$  nucleon-nucleon interaction including three-body forces and relativistic boost corrections [24]. The best fit parameters are  $E_0 = -15.8 \text{ MeV}$ ,  $S_0 = 32 \text{ MeV}$ ,  $\gamma = 0.6$ , and  $\delta = 0.2$ . The EOS from Ref. [24] is considered one of the most reliable ones. In this way possible uncertainties coming from the nucleonic EOS are minimized.

The symmetry energy in dense matter is defined as

$$a_t = \frac{1}{8} \frac{\partial^2 E/A}{\partial x_p^2} \Big|_{\rho_B=\rho_0}. \quad (10)$$

Since there are no hyperons at saturation density we can use Eq. (9) directly to obtain  $a_t = S_0$ . The incompressibility is given by

$$K_0 = 9\rho^2 \frac{\partial^2 E/A}{\partial \rho^2} \Big|_{\rho_B=\rho_0} \quad (11)$$

from which we obtain the relation  $K_0 = -18E_0/(1 + \delta)$ .

To study the impact of the softness of the EOS and the effects of the symmetry energy we vary  $K_0$  and  $a_t$  in a broader interval. From experimental constraints the values for  $K_0$  range between 200 MeV and 300 MeV and those for  $a_t$  between 28 and 36 MeV, see Ref. [25] and references therein. We vary  $K_0$  and  $a_t$  within these limits to study the effects of both parameters on the appearance and concentrations of hyperons in dense matter. While they do not influence the particle concentrations directly, they modify the composition of the matter indirectly by changing the available energy. In this way the point at which hyperons will appear is affected. Results for various values of  $K_0$  are shown in Fig. 3 (in symmetric matter the energy per particle is only sensitive to the incompressibility). In all cases the saturation point is at  $E/A = -16 \text{ MeV}$ . The parameter range allows us to classify the nucleonic EOS as a stiffer ( $K_0 = 300 \text{ MeV}$ ) or a softer ( $K_0 = 200 \text{ MeV}$ ) one.

In addition,  $K_0$  directly influences the maximum allowed mass of a neutron star. By increasing  $K_0$  the energy of the system is increased and, as a consequence, more and more hyperons can be produced. This in turn will decrease the allowed maximum mass of a neutron star. Such a nontrivial connection creates a conundrum: If we use a stiffer nucleonic EOS by increasing  $K_0$  we then allow for higher hyperon concentrations which softens the total EOS.

By means of Eq. (8) we can split the total energy per particle, Eq. (6), into a purely nucleonic part and a remainder  $E'/A$  via

$$E/A = \frac{\rho_N}{\rho_B} E_{NN}/A + E'/A \quad (12)$$

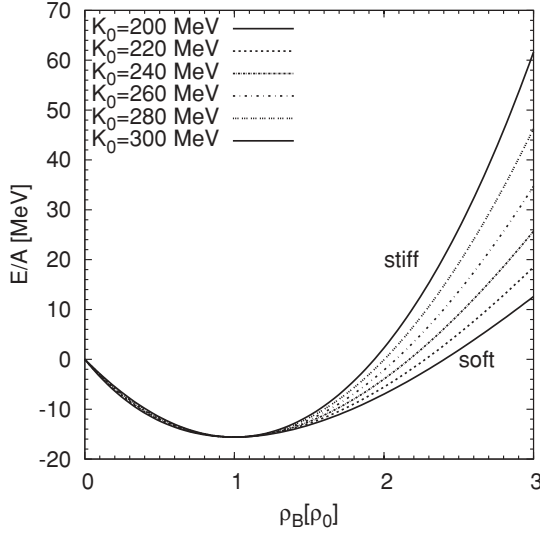


FIG. 3. Parametric EOS in symmetric nuclear matter as obtained from the parametrization of Ref. [23].

with the rest

$$\begin{aligned}
E'/A &= \frac{2}{\rho_B} \sum_N \int_0^{k_{FN}} \frac{d^3 p}{(2\pi)^3} \frac{1}{2} U_N^Y(p) \\
&+ \frac{2}{\rho_B} \sum_Y \int_0^{k_{FY}} \frac{d^3 p}{(2\pi)^3} \left[ M_Y + \frac{p^2}{2M_Y} \right. \\
&\left. + \frac{1}{2} U_Y^N(p) + \frac{1}{2} U_Y^Y(p) \right]. \quad (13)
\end{aligned}$$

In symmetric matter, which is composed only of nucleons,  $E'/A$  vanishes, but with this separation we can calculate the total  $E'/A$  for arbitrary hyperon concentrations. In the following we will calculate the EOS including hyperons by determining their concentrations in  $\beta$  equilibrium.

## IV. $\beta$ EQUILIBRIUM

### A. Composition of matter

In order to determine the threshold densities for hyperons their concentrations are needed. These are fixed by charge neutrality and  $\beta$  equilibrium. The latter refers to the equilibrium under the weak interaction decays

$$B_1 \rightarrow B_2 + l + \bar{\nu}_l, \quad (14)$$

where  $B_1$  and  $B_2$  denote the baryons,  $l \in \{e^-, \mu^-, \tau^-\}$  the negatively charged leptons and  $\bar{\nu}_l$  the corresponding neutrinos. In the case when the neutrinos are not trapped in the star (i.e.,  $\mu_\nu = 0$ ) these requirements amount to

$$0 = \sum_b [\rho_b^{(+)} - \rho_b^{(-)}] + \sum_l [\rho_l^{(+)} - \rho_l^{(-)}] \quad (15)$$

for the charge neutrality and

$$\mu_{\Sigma^-} = \mu_{\Sigma^-} = \mu_n + \mu_e, \quad (16)$$

$$\mu_{\Xi^0} = \mu_{\Lambda} = \mu_{\Sigma^0} = \mu_n, \quad (17)$$

$$\mu_{\Sigma^+} = \mu_p = \mu_n - \mu_e, \quad (18)$$

for the chemical potentials. The densities of positively and negatively charged baryons and leptons are denoted by  $\rho_b^{(\pm)}$  and  $\rho_l^{(\pm)}$ , respectively. The chemical potentials  $\mu$  are labeled by the corresponding particles. In the absence of neutrinos all lepton and antilepton chemical potentials are equal. In addition to the electrons, muons are also present. The  $\tau$  lepton does not appear since it is too heavy.

At zero temperature, the chemical potential of a fermion system is equal to its Fermi energy. For relativistic noninteracting leptons it is given by

$$\mu_l = \sqrt{m_l^2 + k_{F_l}^2} = \sqrt{m_l^2 + (3\pi^2 x_l \rho)^{2/3}} \quad (19)$$

with the corresponding lepton density ratio  $x_l = \rho_l / \rho_L$ . The total lepton density  $\rho_L$  is the sum over all three leptons. For nonrelativistic interacting baryons, the chemical potential for species  $b$  reads

$$\mu_b = M_b + \frac{k_{F_b}^2}{2M_b} + U_b(k_{F_b}). \quad (20)$$

For a given total baryon density  $\rho_B$  the Eqs. (15)–(18) govern the composition of matter, i.e., the baryonic and leptonic concentrations. The corresponding solution is referred to as  $\beta$ -stable matter.

For the sake of consistency we now have to treat the nucleonic part of the chemical potential  $\mu_N$  in the same way as the corresponding energy per particle. Since the chemical potential can be obtained as a derivative of the energy density  $\epsilon$  and is related to the energy per particle via  $\epsilon = \rho_B E/A$ , we use the definition

$$\mu_b = \frac{\partial \epsilon}{\partial \rho_b} \quad (21)$$

to have the appropriate replacement in the nucleonic chemical potential. Finally, we arrive at the expression

$$\mu_N = \frac{\partial \epsilon_{NN}}{\partial \rho_N} + U_N^Y(k_{F_Y}), \quad (22)$$

where we have effectively replaced  $M_N + \frac{k_{F_N}^2}{2M_N} + U_N^N(k_{F_N})$  of Eq. (20) with the derivative  $\partial \epsilon_{NN} / \partial \rho_N$ . In this way the parametrization Eq. (9) enters in the nucleonic part of the chemical potential.

Since we are only parameterizing the nucleonic sector, no such replacement is necessary for the hyperons. However, since we have neglected the  $YY$  interaction  $U_Y^Y(k_{F_Y})$  is zero and Eq. (20) reduces to

$$\mu_Y = M_Y + \frac{k_{F_Y}^2}{2M_Y} + U_Y^N(k_{F_Y}). \quad (23)$$

For the determination of the particle concentration the single-particle potential in equilibrium is used. For hyperons below the threshold density it is given by  $U_Y(p=0)$ , similar to the symmetric matter case. Above the threshold density it depends on composition and density. In Fig. 4 the density dependence of  $U_{\Sigma^-}(k_{F_{\Sigma^-}})$  in  $\beta$  equilibrium for

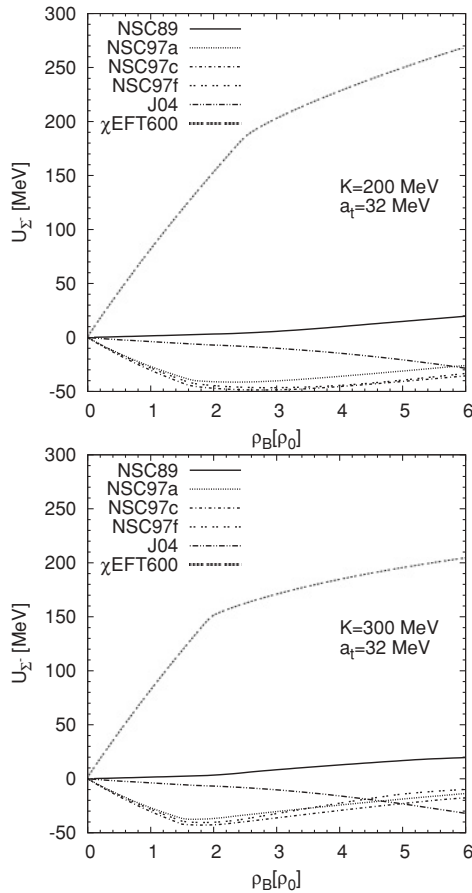


FIG. 4. Density dependence of  $U_{\Sigma^-}(k_{F_{\Sigma^-}})$  for  $\beta$ -equilibrated matter. (Upper panel)  $K_0 = 200$  MeV; (lower panel)  $K_0 = 300$  MeV.

two different incompressibilities  $K_0$  is shown. In the figure a kink in the curves appears at the point where the hyperons appear.

Another observation is the relative ordering and the magnitudes which resemble those of the single-particle potentials at zero momentum in symmetric matter as shown in Fig. 1. Essentially, the NSC97a, NCS97c, NSC97f, and J04 interactions are still slightly attractive while the NSC89 and  $\chi$ EFT600 remain repulsive. Similar observations hold for the  $\Lambda$  system. A new structure in form of a second inflection point emerges due to the appearance of the  $\Sigma^-$  hyperon.

A better indicator at which densities hyperons start to appear is given by the concentrations of all particles and is displayed in Figs. 5 and 6. In Fig. 5 a “soft” nucleonic EOS is used in combination with an attractive  $\Lambda N$  and a very repulsive  $\Sigma N$  interaction implemented by the  $\chi$ EFT600 model. In contrast in Fig. 6 a “stiff” EOS is used represented by the NSC97f model which has a similar  $\Lambda N$  interaction compared to the  $\chi$ EFT600 model but also an attractive  $\Sigma N$  interaction. This difference already leads to very different density profiles. While in Fig. 5 the  $\Lambda$  hyperon is the first one which appears and no  $\Sigma^-$  hyperons are present, the  $\Sigma^-$  hyperon appears first in Fig. 6.

One should note that with the appearance of the  $\Sigma^-$  hyperon the density of the negatively charged leptons starts to drop immediately. This is because their role in the charge neutrality

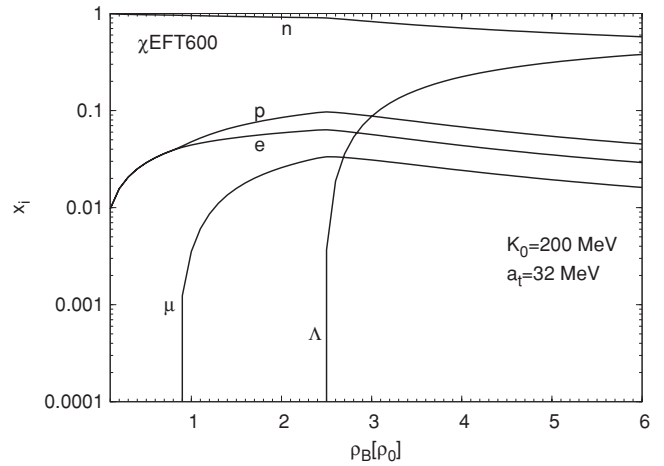


FIG. 5. Density ratios for different particles for a “soft” nucleonic EOS as a function of the baryon density using the  $\chi$ EFT600 model.

condition, Eq. (15), is now being taken over by the  $\Sigma^-$ . Similarly, the appearance of the  $\Lambda$  hyperon will accelerate the disappearance of neutrons since both are neutral particles.

Once the composition of the matter has been determined by demanding  $\beta$  equilibrium we can calculate the energy per particle. For this purpose, we cannot use Eq. (6) but have to use Eqs. (12) and (9). The result is presented in Fig. 7 where the energy per particle in  $\beta$ -stable matter is shown as a function of the density for different  $YN$  models. The symmetry energy is fixed to  $a_t = 32$  MeV while the incompressibility is set to  $K_0 = 200$  MeV (upper panel in the figure) and to  $K_0 = 300$  MeV (lower panel). In addition, the EOS with hyperons is compared with the purely nucleonic one.

One easily observes the onset of the hyperon appearance at the point at which the curves start to deviate. As expected the differences between the various  $YN$  interactions do not modify the EOS for very small densities. In the range between  $(2 - 3)\rho_0$ , all EOS’s are similar to each other. However, for increasing densities the influence of hyperons becomes more significant, resulting in rather different EOS’s. This concerns not only the magnitudes of the different energies

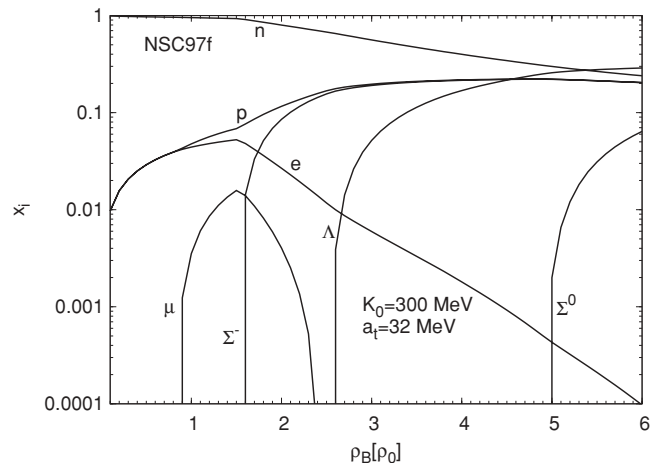


FIG. 6. Same as Fig. 5 but for “stiff” nucleonic EOS using the NSC97f model.

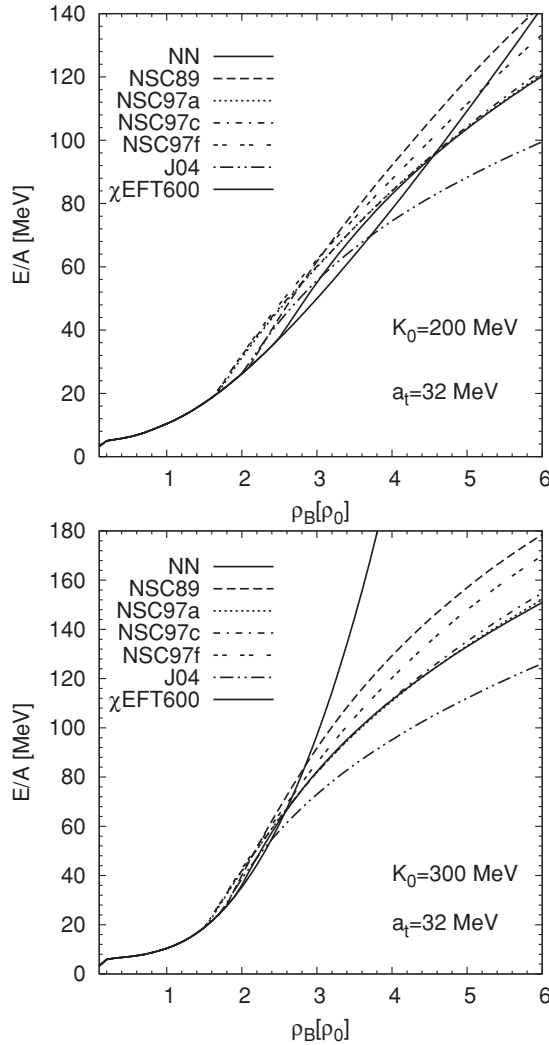


FIG. 7. Various EOS for  $\beta$ -equilibrated matter for two different  $K_0$  as a function of density. (Upper panel) Soft EOS; (lower panel) stiff EOS.

per particle but also their slopes at higher densities. These variations will lead to differences in the pressure and finally to significant changes in the possible maximum mass of a neutron star.

### B. Threshold densities

The appearance of a given hyperon species is determined by increasing the density for fixed  $K_0$  and  $a_t$ . The resulting threshold densities for the  $\Sigma^-$  hyperon for certain  $K_0$  and  $a_t$  are collected in Fig. 8 for six different  $YN$  interactions. Similarly, the threshold densities for the  $\Lambda$  hyperon are shown in Fig. 9. From these figures one sees how the single-particle potentials for various  $YN$  interactions modify the threshold densities. In this way, the properties of the  $YN$  interaction in Fig. 1 and Fig. 2 can be attributed to the hyperon appearances.

From Fig. 8 one concludes that the  $\Sigma^-$  hyperon appears between  $1.4\rho_0$  and  $2.4\rho_0$  with the exception of the  $\chi$ EFT600

model. For almost all  $YN$  interactions used in the present study the  $\Sigma^-$  is the first hyperon which will appear even though the  $\Lambda$  hyperon is the lighter one. The reason is that the heavier mass of the  $\Sigma^-$  is offset due to the presence of the  $e^-$  chemical potential, cf. Eq. (16). In general, heavier and more positively charged particles appear later. In the case of the  $\Sigma^-$ , compared to the  $\Lambda$ , the effect caused by the electric charge dominates the one coming from the mass in almost all cases. For the  $\Sigma^-$  hyperon a further modification caused by the electric charge, is the influence of  $a_t$  on the threshold density because the electron chemical potential is modified by the symmetry energy. Thus, the decrease of the threshold densities due to the increase of  $K_0$  is analogous to the increase due to  $a_t$ .

For the  $\Lambda$  hyperon the range of threshold densities is between densities from  $1.7\rho_0$  to  $4.5\rho_0$  depending on the choice of  $K_0$ ,  $a_t$ , and the  $YN$  interaction used, cf. Fig. 9. The influence of  $K_0$  on the threshold density for this hyperon is larger than the one from  $a_t$ . This is reasonable since  $K_0$  controls the rate of the energy increase with the density more directly, while  $a_t$  affects only the details of the  $\beta$  equilibrium. One clearly recognizes in Fig. 9 that the  $\Lambda$  appears earlier for larger incompressibilities. Thus, in general we see that for increasing  $K_0$  the threshold densities decrease for both hyperons.

In contrast to the previous  $K_0$  and  $a_t$  discussion, the influence of the single-particle potentials on the threshold densities is harder to analyze.

The threshold densities for the  $\Sigma^-$  are largest for the  $\chi$ EFT600 interaction which yields the most repulsive  $\Sigma^-$  single-particle potential. In general, hyperons will appear earlier for a more attractive single-particle potential. This becomes obvious from Eq. (20): the chemical potential decreases for a more negative  $U_b(k_{F_b})$  and, consequently, the threshold density will also decrease. Thus, the most repulsive single-particle potential like the one for the  $\chi$ EFT600 leads to the largest threshold density. For the  $\Lambda$  hyperon the threshold densities are smallest for the most attractive single-particle potential obtained with the J04 model, cf. Fig. 9. On the other hand, they are largest for the most repulsive NSC89 interaction. For the NSC97f interaction, which is between these extremes, the  $\Lambda$  threshold densities are very close to those of the most repulsive NSC89 one, cf. Fig. 9. This stems from the appearance of the  $\Sigma^-$  hyperon. The effect is caused by the slowdown of the increase of the neutron chemical potential and is further related to the rapid increase of the  $\Sigma^-$  density just after its appearance, cf. Fig. 6. Basically, the slowdown occurs as soon as a new hyperon appears because most of the energy is used for its creation. Once the concentration of the hyperon has reached a plateau, the neutron chemical potential resumes its increase until a further hyperon might appear. Thus, the appearance of the first hyperon shifts the threshold density of the next hyperon toward higher values. This effect explains why the threshold densities of the  $\Lambda$  are so similar for the NSC97f and NSC89 interactions. It also makes clear why the  $\Lambda$  threshold densities for the  $\chi$ EFT600 interaction are smaller than those of the NSC97a, NSC97c, and NSC97f interactions even though their  $\Lambda$  single-particle potentials are almost the same, cf. Fig. 1. In the case of the J04 model the delay mechanism described above becomes very interesting. For this  $YN$  interaction the  $\Lambda$  and  $\Sigma^-$  hyperon appear almost

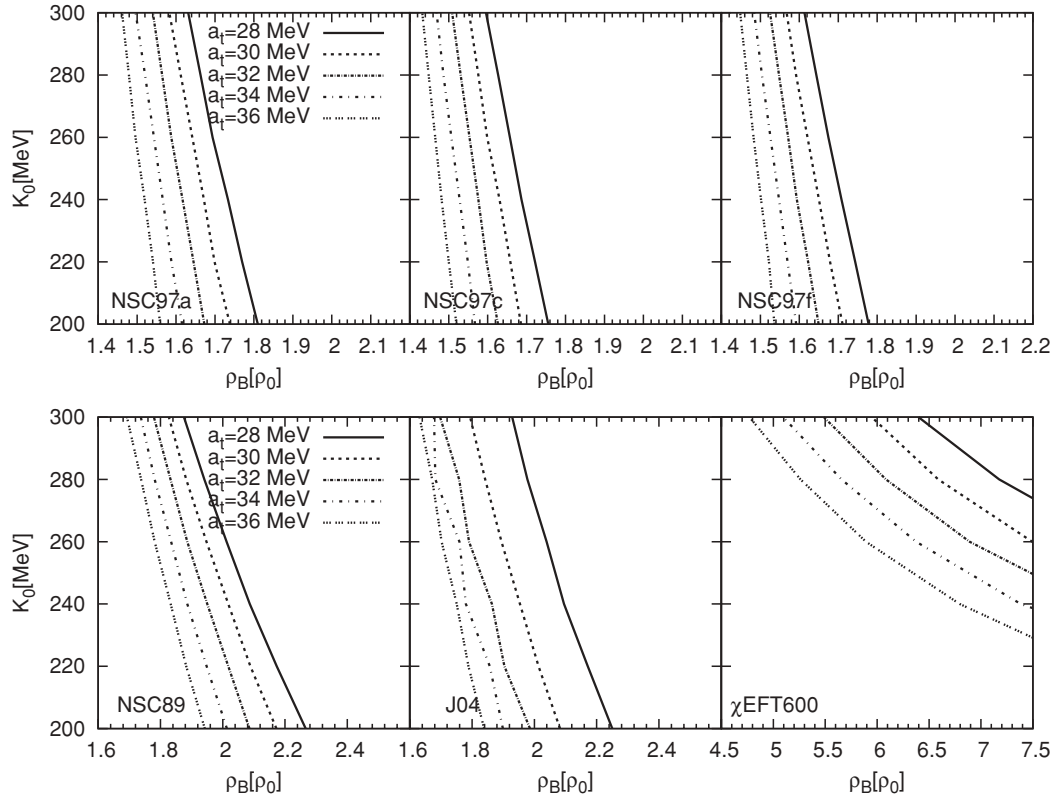


FIG. 8. Threshold densities for the  $\Sigma^-$  hyperon with various incompressibilities  $K_0$  and symmetry energy  $a_1$  for six different YN interactions.

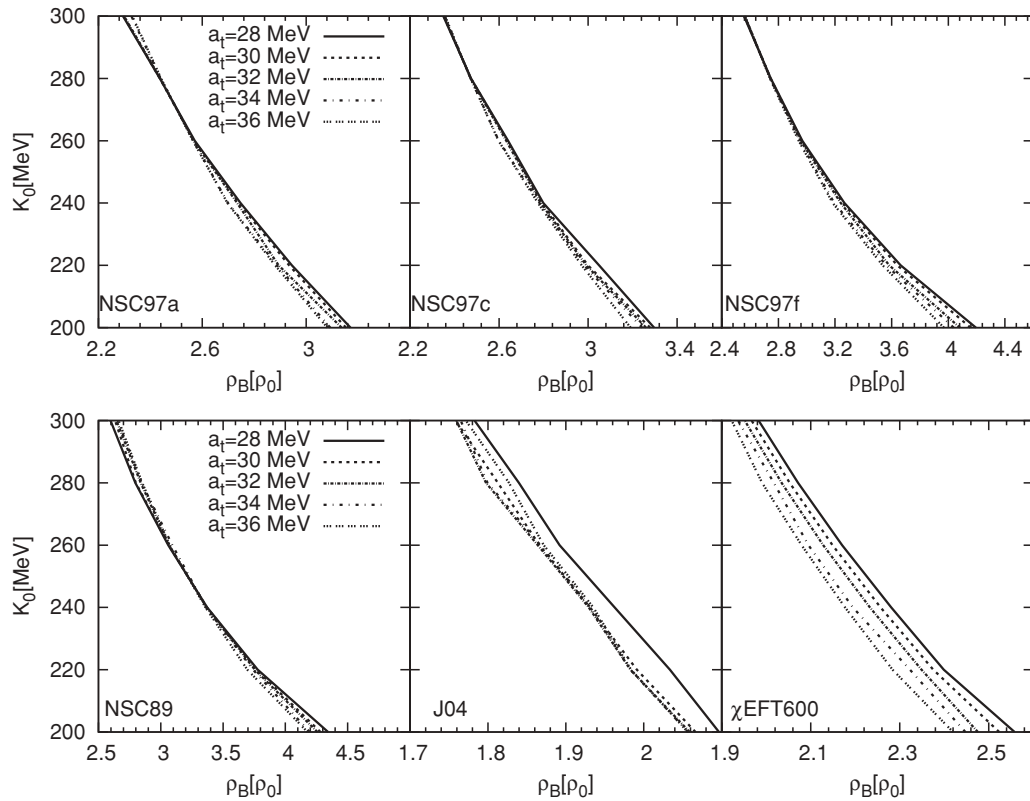


FIG. 9. Threshold densities for the  $\Lambda$  hyperon similar to Fig. 8.

at the same density. In this case the neutron chemical potential stagnates but the  $\Lambda$  and the  $\Sigma^-$  single-particle potentials are attractive enough to compensate for this.

To summarize this section strangeness appears around  $\sim 2\rho_0$  for all  $YN$  models and parameter sets used. Note, that the appearance of the first hyperon, whether it is the  $\Sigma^-$  or the  $\Lambda$ , cannot be altered by taking into account  $YY$  interactions which have been neglected in this work. The present study in terms of the broad parameter ranges as well as the multitude of  $YN$  interaction models reveals that strangeness in the interior of neutron stars cannot be ignored. Similar conclusions are obtained in the Brueckner-Hartree-Fock theory [26].

## V. STRUCTURE OF NEUTRON STARS

In this section we analyze the effect of the EOS including hyperons on neutron stars. We focus on non-rotating stars, ignoring any changes, caused by the rotation. For a given EOS, the mass-radius relation of a NS can be determined by solving the familiar Tolman-Oppenheimer-Volkoff equation (TOV) [27]. To describe the outer crust and atmosphere of the star, i.e., the region of subnuclear matter densities for very small baryon densities below  $\rho_B < 0.001 \text{ fm}^{-3}$ , we have used the EOS of Baym, Pethick, and Sutherland [28], which relies on properties of heavy nuclei. For densities between  $0.001 \text{ fm}^{-3} \leq \rho_B \leq 0.08 \text{ fm}^{-3}$ , i.e., for the inner crust, we have used the EOS of Negele and Vautherin [29], who have performed Hartree-Fock calculations of the nuclear crust composition. Details on crust properties can be found, e.g., in Refs. [30,31], while recent state-of-the-art approaches are discussed in Ref. [32].

In Fig. 10 the mass-radius relation of a NS for a soft EOS (left panel) and for a stiff EOS (right panel) is shown. The symmetry energy  $a_t = 32 \text{ MeV}$  is kept fixed in both

calculations and the resulting mass-radius relation without any strangeness is also added for comparison.

As can be seen from the figure the appearance of hyperons reduces the NS mass drastically compared with the pure  $NN$  case. Even for larger values of the incompressibility, i.e.,  $K_0 = 300 \text{ MeV}$ , the maximum mass, obtained with all  $YN$  interactions used, is still below the largest precisely known and measured NS masses  $1.44 M_\odot$  of the Hulse-Taylor binary pulsar. This is not an unusual result and is also seen in other, related works such as, e.g., Refs. [8,33–35]. In general, any inclusion of further degrees of freedom to the nucleons will reduce the NS mass.

Due to large uncertainties in the high density behavior of the symmetry energy we investigate its influence on the NS masses as follows: The parameter  $\gamma$  in Eq. (9) determines the symmetry energy changes, i.e., how asy-stiff or asy-soft the EOS is. The value of  $\gamma = 0.6$ , used so far, represents an asy-soft system [36]. Above saturation density we change the value of this parameter and use  $\gamma = 1$  while keeping all other parameters fixed representing a asy-stiff system. The effect of the  $\gamma$  modification is shown in Fig. 11.

Only small changes in the mass-radius relation are obtained when hyperons are included. In most cases the mass difference is  $0.1 M_\odot$ . An increasing  $\gamma$  leads to an increase in the proton concentration which in turn leads to an increase in the  $\Sigma^-$  concentration. This largely cancels any energy gain from an increased symmetry energy term that could possibly increase the mass of a neutron star. The biggest mass change is seen for  $K_0 = 200 \text{ MeV}$  with the  $\chi$ EFT600 interaction since this model does not contain any  $\Sigma^-$  hyperons. However, even in this case the difference is below  $0.2 M_\odot$  which leads to a maximum mass below  $1.2 M_\odot$ . A more noticeable change can be observed for the radius. A radius shift of 1 km toward larger radii is seen for all curves. Furthermore, if we in addition vary  $a_t$  at saturation density between 28 and 36 MeV, a less pronounced effect on the NS mass is visible as compared to the variation of  $\gamma$ .

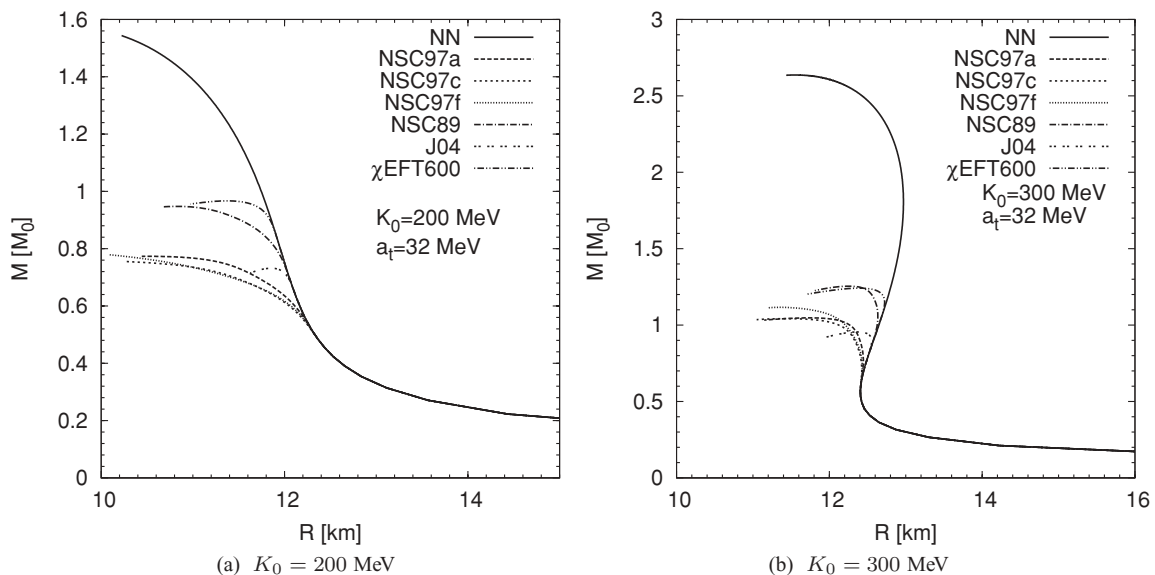


FIG. 10. Mass-radius relation of a neutron star for symmetry energy  $a_t = 32 \text{ MeV}$  and different  $YN$  interactions. For comparison the mass-radius curve obtained for the pure  $NN$  interaction is also shown. (Left panel) Soft EOS; (right panel) stiff EOS.

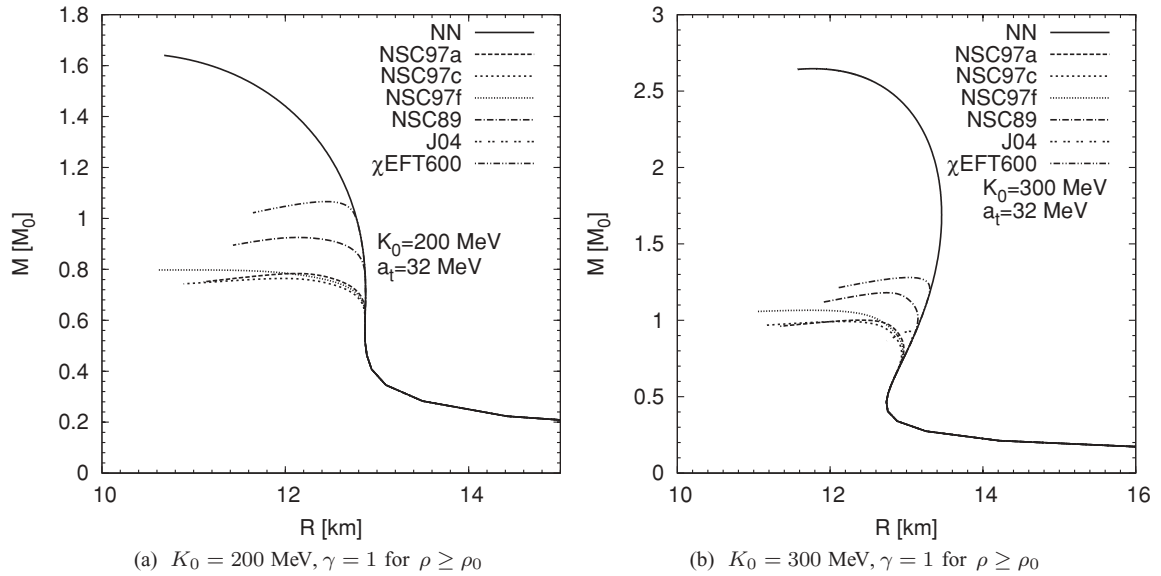


FIG. 11. Mass-radius relation of a neutron star for symmetry energy  $a_t = 32$  MeV,  $\gamma = 1$  for  $\rho \geq \rho_0$  and different  $YN$  interactions. For comparison the mass-radius curve obtained for the pure  $NN$  interaction is also shown. (Left panel) Soft EOS; (right panel) stiff EOS.

To complete our investigation of hyperon effects on the neutron star EOS we also need to consider modifications induced by the  $YY$  and  $\Xi N$  interactions. In order to evaluate the effects of the  $S = -2$  sector we have to construct  $YY$  and  $\Xi N$   $V_{\text{low } k}$  interactions, along the lines discussed earlier for the  $S = -1$  sector. Obviously, since there are more particles to consider, the situation complicates considerably from a numerical point of view. Unfortunately, unlike the  $S = -1$  sector where we had several different “bare” interactions from which we constructed the  $V_{\text{low } k}$  potentials, in the  $S = -2$  sector we only have one, namely the NSC97 interaction. We also note that the inclusion of the  $S = -2$  sector will not

influence the appearance of the first hyperon. Hence we have neglected the  $S = -2$  up to this point.

Figure 12 shows the mass-radius relation of a NS with different  $YN$ ,  $YY$ , and  $\Xi N$  interactions is presented. The effect of the inclusion of the  $S = -2$  sector is rather marginal. As is visible in Fig. 12 the maximum masses are lower than in the previous cases which is reasonable since a further degree of freedom, the  $\Xi$  particle, is added. However, we note that the NSC97  $YY$  interaction is attractive which is the reason for the decrease of the allowed maximum NS masses, see, e.g., Ref. [8]. A repulsive  $YY$  interaction would have an opposite effect as shown in Ref. [34].

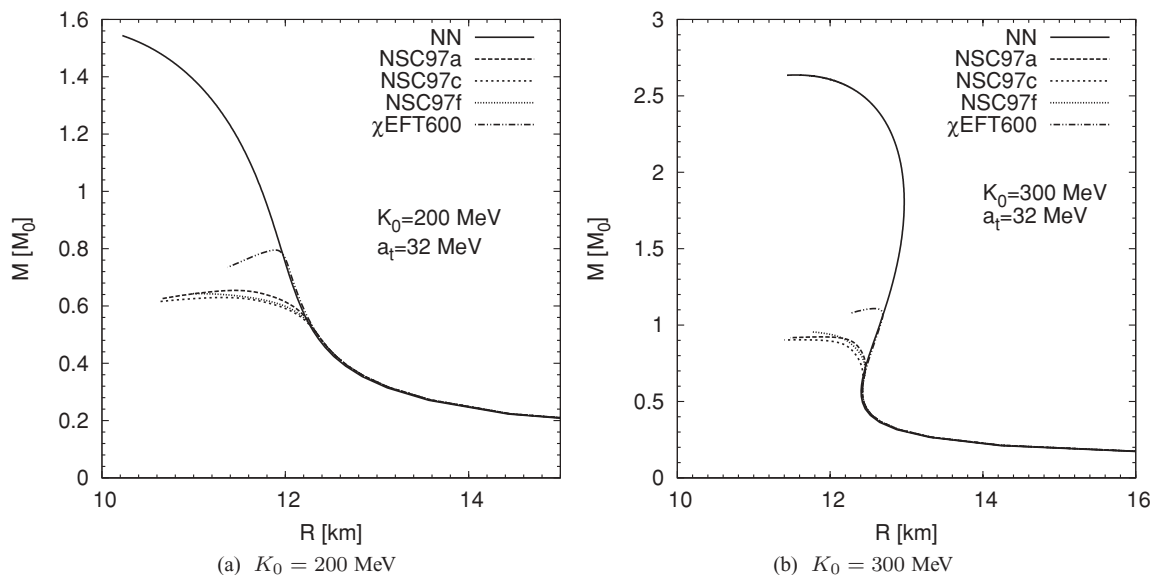


FIG. 12. Mass-radius relation of a neutron star for symmetry energy  $a_t = 32$  MeV and different  $YN$ ,  $YY$ , and  $\Xi N$  interactions. For comparison the mass-radius curve obtained for the pure  $NN$  interaction is also shown. (Left panel) Soft EOS; (right panel) stiff EOS.

It is also interesting to point out that for the  $\chi$ EFT600 interaction, where the  $\Sigma^-$  hyperons appears late, if at all, it is the  $\Xi$  hyperons which takes its pace and influences the maximum mass of a NS [37,38]. For all other models in which the  $\Sigma^-$  appears earlier than the  $\Xi$  their influence on the NS mass is marginal.

## VI. SUMMARY AND CONCLUSIONS

The main intention of the present work was to study the consequences of available hyperon-nucleon interactions on the composition of neutron stars and the maximum masses. The analysis was performed in the framework of the renormalization group improved  $V_{\text{low } k}$  interaction deduced from available bare potentials. Since the experimental data base is very limited, these potentials are not well constrained, in contrast to the nucleon-nucleon case.

We have determined the threshold densities for the appearance of hyperons in  $\beta$ -equilibrated neutron star matter to lowest order in a loop expansion. To explore the sensitivity to available  $YN$  potentials we have constructed single-particle potentials for the  $\Lambda$  and  $\Sigma^-$  hyperon in lowest order and deduced the energy per particle. We have replaced the pure nucleonic contribution to the energy per particle by an analytic parametrization. This replacement enables us to vary the incompressibility  $K_0$  and symmetry energy  $a_t$  of the purely nucleonic EOS and to investigate their influence on the threshold densities of hyperons. The composition of  $\beta$ -stable matter has been determined by the requirement of charge neutrality and  $\beta$  equilibrium. The corresponding threshold densities for various values of  $K_0$  and  $a_t$  were evaluated. The most important conclusion is that a more attractive single-particle potential will decrease the chemical potential and thus decrease the threshold density of the corresponding hyperon.

We have found that, irrespective of the  $YN$  interactions, incompressibility, and symmetry parameter used, hyperons will appear in dense neutron star matter at densities around  $\sim 2\rho_0$ . This inevitably leads to a significant softening of the EOS which in turn results in smaller maximum masses of a neutron star compared to a purely nucleonic EOS. Notably,

the predicted maximum masses are well below the observed value of  $1.4 M_\odot$ , an outcome also known from other works, e.g., Refs. [8,33–35]. This poses a serious problem.

The softening of the EOS due to hyperons cannot be circumvented by stiffening the nucleonic EOS, i.e., by increasing  $K_0$ , since this will cause hyperons to appear earlier. Changing the high-density behavior of the symmetry energy dependence or including the  $S = -2$  sector does not alter this conclusion either. For more details about the  $S = -2$  sector, in particular  $\Xi$  hyperons in dense baryonic matter see, e.g., Refs. [39–42]. This can only mean that correlations beyond the one-loop level could be important to stiffen the hyperon contributions to the EOS. This, however, is not sufficient, as Brueckner-Hartree-Fock calculations indicate [9,26]. As has been known for a long time from nonrelativistic nuclear many-body theory, three-body interactions are crucial to yield a stiff nucleonic EOS. Repulsive three-body forces may also play a role in the hyperon sector. There is, however, little empirical information available at present. There is also the possibility of an early onset of quark-hadron transition to cold quark matter. This might also stiffen the high-density equation of state.

Clearly, our results pose significant restrictions on any reasonable equations of state employed in the study of neutron star matter. With the prediction of a low onset of hyperon appearance it becomes mandatory to seriously consider strangeness with respect to neutron stars. Even though our predictions for the maximum masses of neutron stars are too low, the treatment of hyperons in neutron stars is necessary and any approach to dense matter must address this issue.

## ACKNOWLEDGMENTS

H.D. was partially supported by the Helmholtz Gemeinschaft under Grant VH-VI-041 and by the Helmholtz Research School for Quark Matter Studies. B.J.S. acknowledges support by the BMBF under Grant 06DA123 and J.W. from the Extreme Matter Institute within the Helmholtz Alliance “Cosmic Matter in the Laboratory.” This work was also supported in part by the Grant SFB634 of the Deutsche Forschungsgemeinschaft. We thank R. Alkofer and M. Oertel for critical reading of the manuscript.

- 
- [1] M. Prakash *et al.*, Phys. Rep. **280**, 1 (1997).
  - [2] K. Strobel, C. Schaab, and M. K. Weigel, Astron. Astrophys. **350**, 497 (1999).
  - [3] V. A. Ambartsumyan and G. S. Saakyan, Sov. Astron. **4**, 187 (1960).
  - [4] J. Schaffner and I. N. Mishustin, Phys. Rev. C **53**, 1416 (1996).
  - [5] V. R. Pandharipande, Nucl. Phys. A **178**, 123 (1971).
  - [6] N. K. Glendenning, Astrophys. J. **293**, 470 (1985).
  - [7] W. Keil and H. T. Janka, Astron. Astrophys. **296**, 145 (1995).
  - [8] I. Vidana, A. Polls, A. Ramos, L. Engvik, and M. Hjorth-Jensen, Phys. Rev. C **62**, 035801 (2000).
  - [9] M. Baldo, G. F. Burgio, and H. J. Schulze, Phys. Rev. C **61**, 055801 (2000).
  - [10] T. A. Rijken, V. G. J. Stoks, and Y. Yamamoto, Phys. Rev. C **59**, 21 (1999).
  - [11] B.-J. Schaefer, M. Wagner, J. Wambach, T. T. S. Kuo, and G. E. Brown, Phys. Rev. C **73**, 011001(R) (2006).
  - [12] M. Wagner, B.-J. Schaefer, J. Wambach, T. T. S. Kuo, and G. E. Brown, Phys. Rev. C **74**, 054003 (2006).
  - [13] H. Djapo, B.-J. Schaefer, and J. Wambach, Eur. Phys. J. A **36**, 101 (2008).
  - [14] P. M. M. Maessen, T. A. Rijken, and J. J. de Swart, Phys. Rev. C **40**, 2226 (1989).
  - [15] J. Haidenbauer and Ulf-G. Meißner, Phys. Rev. C **72**, 044005 (2005).
  - [16] H. Polinder, J. Haidenbauer, and U.-G. Meißner, Nucl. Phys. A **779**, 244 (2006).

- [17] P. F. Bedaque and U. van Kolck, *Ann. Rev. Nucl. Part. Sci.* **52**, 339 (2002).
- [18] E. Epelbaum, *Prog. Part. Nucl. Phys.* **57**, 654 (2006).
- [19] R. J. Furnstahl, G. Rupak, and T. Schäfer, *Ann. Rev. Nucl. Part. Sci.* **58**, 1 (2008).
- [20] A. L. Fetter and J. D. Walecka, *Quantum Theory Of Many-Particle Systems* (McGraw-Hill, New York, 1971).
- [21] H.-J. Schulze, M. Baldo, U. Lombardo, J. Cugnon, and A. Lejeune, *Phys. Rev. C* **57**, 704 (1998).
- [22] I. Vidana, A. Polls, A. Ramos, and H.-J. Schulze, *Phys. Rev. C* **64**, 044301 (2001).
- [23] H. Heiselberg and M. Hjorth-Jensen, *Phys. Rep.* **328**, 237 (2000).
- [24] A. Akmal, V. R. Pandharipande, and D. G. Ravenhall, *Phys. Rev. C* **58**, 1804 (1998).
- [25] J. M. Lattimer and M. Prakash, *Phys. Rep.* **442**, 109 (2007), arXiv:astro-ph/0612440.
- [26] M. Baldo, G. F. Burgio, and H. J. Schulze, *Phys. Rev. C* **58**, 3688 (1998).
- [27] J. R. Oppenheimer and G. M. Volkoff, *Phys. Rev.* **55**, 374 (1939).
- [28] G. Baym, C. Pethick, and P. Sutherland, *Astrophys. J.* **170**, 299 (1971).
- [29] J. W. Negele and D. Vautherin, *Nucl. Phys. A* **207**, 298 (1973).
- [30] C. J. Pethick and D. G. Ravenhall, *Ann. Rev. Nucl. Part. Sci.* **45**, 429 (1995).
- [31] P. Haensel, in *Physics of Neutron Star Interiors*, Lecture Notes in Physics, Vol. 578, edited by D. Blaschke, N. K. Glendenning, and A. Sedrakian (Springer-Verlag, Heidelberg, 2001), p. 127.
- [32] S. B. Ruster, M. Hempel, and J. Schaffner-Bielich, *Phys. Rev. C* **73**, 035804 (2006).
- [33] J. Schaffner-Bielich, M. Hanauske, H. Stöcker, and W. Greiner, *Phys. Rev. Lett.* **89**, 171101 (2002).
- [34] L. Mornas, *Eur. Phys. J. A* **24**, 293 (2005).
- [35] J. Schaffner-Bielich, S. Schramm, and H. Stöcker (2007), arXiv:0711.2639.
- [36] H. H. Wolter, V. Prassa, G. Lalazissis, T. Gaitanos, G. Ferini, M. Di Toro, and V. Greco, *Prog. Part. Nucl. Phys.* **62**, 402 (2009).
- [37] N. K. Glendenning, *Phys. Rev. C* **64**, 025801 (2001).
- [38] S. Balberg, I. Lichtenstadt, and G. B. Cook (1998), arXiv:astro-ph/9810361.
- [39] P. Wang, S. Lawley, D. B. Leinweber, A. W. Thomas, and A. G. Williams, *Phys. Rev. C* **72**, 045801 (2005).
- [40] S. Pal, M. Hanauske, I. Zakout, H. Stocker, and W. Greiner, *Phys. Rev. C* **60**, 015802 (1999).
- [41] H. Huber, F. Weber, M. K. Weigel, and C. Schaab, *Int. J. Mod. Phys. E* **7**, 301 (1998).
- [42] N. K. Glendenning, *Phys. Lett. B* **114**, 392 (1982).